Geof. Int. Vol. 20-1, 1981, pp. 11-39.

MODEL OF MID- AND LOW-LATITUDE F REGION IONOSPHERE AND PROTONOSPHERE

A. TAN*
S. T. WU*
(Received: Jul. 3, 1981)

RESUMEN

En este trabajo se resuelven las ecuaciones combinadas de continuidad y momentum de los iones O^+ y H^+, en la región F y la protonosfera, para una estación de latitud media (Arecibo) y una estación de latitud baja (Jicamarca) con el fin de investigar el comportamiento diurno de la densidad electrónica máxima N_mF2, la altura del pico H_mF2, el nivel de transición $O^+ - H^+$, o sea H_{tr} y el nivel de transición de densidad N_{tr}. Los efectos del viento neutral sobre las curvas N_mF2, H_mF2, N_{tr} y H_{tr}, sobre Arecibo son más importantes y generalmente en dirección opuesta a los de una desviación electromagnética sinusoidal. La desviación electromagnética desempeña un papel de largo alcance en la formación de los perfiles ionosférico y protonosférico en Jicamarca. Un desvío ascendente que alcanza su máximo durante el día produce un 'valle' en la curva N_mF2, mientras que un desvío ascendente que se mantiene constante durante la mayor parte del día produce una 'meseta'. La depresión nocturna en la curva N_mF2 es debida a los efectos combinados de un lento desvío descendente y de la recombinación química. Una elevación nocturna en N_mF2 es debida a un desvío descendente suficientemente prolongado cuando la 'compresión' resultante de los tubos de campo supera la tasa de pérdida de O^+. Las variaciones diurnas en H_mF2 y en H_{tr} tienden a seguir las del patrón de velocidad de desvío ascendente, con gradientes algo atenuados. Una inversión descendente del desvío a la puesta del Sol produce un aumento en la curva N_{tr} post-crepuscular.

Finalmente, queda demostrada la aplicabilidad del modelo para el estudio de las mediciones totales de contenido electrónico en los experimentos con el radio-faro ATS-6 en Ootacamund. Mediante la comparación con los valores observados, se determinan las probables velocidades de desvío sobre Ootacamund para Octubre y Diciembre de 1975. Los patrones de velocidad de desvío muestran amplias similitudes con los observados sobre Jicamarca.

* *School of Science and Engineering, The University of Alabama in Huntsville, Huntsville, AL 35899 - U. S. A.*

ABSTRACT

The coupled continuity and momentum equations of O^+ and H^+ ions in the F region and the protonosphere are solved for a mid-latitude station (Arecibo) and a low-latitude station (Jicamarca) to investigate the diurnal behavior of the peak electron density N_mF2, the height of the peak H_mF2, the O^+-H^+ transition height H_{tr} and the transition level ion density N_{tr}. The effects of the neutral wind on the N_mF2, H_mF2, N_{tr} and H_{tr} curves above Arecibo are more important than and generally in the opposite direction of those of a sinusoidal electromagnetic drift. The electromagnetic drift plays a far-reaching role in shaping the ionospheric and protonospheric profiles at Jicamarca. An upward drift that peaks during the day produces a 'valley' in the N_mF2 curve, while an upward drift that stays constant during most of the day produces a 'plateau'. The nighttime decay in N_mF2 is due to the combined effects of a slow downward drift and chemical recombination. A nocturnal increase in N_mF2 is due to a sufficiently large downward drift when the resultant 'squeezing' of the field tubes overcomes the O^+ loss rate. The diurnal variations of H_mF2 and H_{tr} tend to follow that of the upward drift velocity pattern, with gradients somewhat smoothed. A downward reversal of the drift at sunset causes an enhancement in the post-sunset N_{tr}.

Finally, the applicability of the model to the study of the total electron content measurements of the ATS-6 radio beacon experiments at Ootacamund is demonstrated. By comparing with the observed values, the probable drift velocities over Ootacamund are determined for October and December, 1975. The drift velocity patterns show broad similarities with those observed over Jicamarca.

1. INTRODUCTION

Ionospheric modelling is a useful device in studying, analyzing and understanding various aspects of the ionosphere. The existing ionospheric models can be classified into two basic categories. First, models of the low-latitude F region ionosphere have been presented by several authors featuring the effect of the east-west electric field in producing the equatorial anomaly. The works of Bramley and Peart (1965), Hanson and Moffett (1966) and Sterling *et al.* (1969) are notable among them. The model of Anderson (1973) incorporates a tilted dipole approximation of the geomagnetic field that is particularly useful in explaining the differences in the F region between the Asian and American sectors. The second category of models is concerned chiefly with the exchange of ionization between the ionosphere and the protonosphere. This is relevant to the mid-latitude regions where the effects of the neutral wind also becomes important. The works of Mayr *et al.* (1972), Moffett and Murphy (1973) and Massa (1974) are worth mentioning in this regard. The two classes of models, although useful in their respective domains of applicability, possess certain limitations. The former is restricted to the low-latitude F regions only and cannot be used to study the overlying protonosphere. The latter class, on the other hand, is suitable for mid-latitude regions only, since electromagnetic drift effects are not included.

The present model is a combination of the two and is generally applicable to both mid- and low-latitude F region and protonosphere. The governing equations of O^+ and H^+ are solved along geomagnetic field lines from the base of the F region in the northern hemisphere to the conjugate point in the southern hemisphere. The effects of the centrifugal force, neutral wind and electromagnetic drift are included. The inclusion of the centrifugal force becomes important for the longer field lines and low-latitude locations (cf. Angerami and Thomas, 1964). For greater accuracy, a more realistic tilted dipole model of the geomagnetic field is incorporated. Thus, distinction is made between the geographic and dipole coordinates as well as between local time and dipole time. In this paper, results of the applications of this model to the ionospheric profiles at a mid-latitude station (Arecibo) and a low-latitude station (Jicamarca) are presented. The model is further used to study the total columnar content from Ootacamund to the ATS-6 satellite as measured by the radio beacon experiments of the satellite.

2. EQUATIONS

The production, loss and movement of ionization are governed by the continuity and momentum equations. The momentum equations of the ions ($O^+$and H^+) and electrons are substituted into the continuity equations of the ions to form two coupled nonlinear partial differential equations called diffusion equations. The various symbols used in this paper are as defined in the Appendix. The indications of the subscripts are as follows: e following T indicates electron and i following T indicates ion. Elsewhere, i stands for the ion under consideration (O^+ or H^+), j stands for the other ion (H^+ or O^+) and n denotes the neutrals. The subscripts || and $\perp$ refer to directions parallel with and perpendicular to the magnetic field. The continuity equation for ions is given by

$$\frac{\partial N_i}{\partial t} = \alpha_i - \beta_i N_i - \nabla \cdot (N_i V_i) \tag{1}$$

By resolving V_i into components along and perpendicular to the field lines, equation (1) can be written as

$$\frac{dN_i}{dt} + N_i \nabla \cdot v_\perp + B \frac{\partial}{\partial s} \left(\frac{N_i V_{i||}}{B} \right) = \alpha_i - \beta_i N_i , \tag{2}$$

where the first term represents the rate of change of N_i in a frame of reference moving with the tube of ionization under the action of the $E \times B$ drift.

Taking into account the pressure gradient forces, gravity, centrifugal force, elec-

tric forces of charge separation and collisional forces, the force equation of the ions, resolved along the field lines is given by

$$\frac{1}{N_i}\frac{\partial P_i}{\partial s} = m_i g_{||} + m_i f_{||} + eE_{||} - \sum_n m_i \nu_{in}(V_{i||} - U_{||}) - m_i \nu_{ij}(V_{i||} - V_{j||}). \quad (3)$$

Since the mass of the electron is negligible compared to that of the ions, the force equation of the electron, resolved along s, can be taken as

$$\frac{1}{N_e}\frac{\partial P_e}{\partial s} = - eE_{||} . \quad (4)$$

Equations (2), (3) and (4), together with the charge neutrality condition, are combined into the diffusion equations for the ions,

$$\frac{dN_i}{dt} = P_i' \frac{\partial^2 N_i}{\partial s^2} + Q_i' \frac{\partial N_i}{\partial s} + R_i' N_i + S_i', \quad (5)$$

where the coefficients are as given in the Appendix.

After Kendall (1962) and Sterling *et al.* (1969), it has been found convenient to make two transformations of the independent variable as follows:

$$q = - \frac{\cos\theta \, \mathrm{cosec}^4\theta}{L^2} , \quad (6)$$

and

$$x = - \frac{\sinh(\Gamma q)}{\sinh(\Gamma q_{min})} , \quad (7)$$

where L is McIlwain's shell parameter, θ the dipole colatitude and Γ is an adjustable parameter. Under these transformations, the diffusion equation (5) is rewritten as

$$\frac{\partial N_i}{dt} = P_i \frac{\partial^2 N_i}{dx^2} + Q_i \frac{\partial N_i}{\partial x} + R_i N_i + S_i , \quad (8)$$

where the coefficients are again found in the Appendix. Equation (8) is solved by the Laasonen (1949) method using the algorithm of Richtmyer (1957).

3. INPUT DATA

The chemical reactions and their rate coefficients used in this study are given in Table 1. Table 2 lists the various collision frequencies. Model electron temperatures showing the broad features of observed diurnal, seasonal, latitudinal and altitudinal variations are prescribed by the following expressions.

$$\text{Day} \qquad T_e(z) = 2000\,[1 + .3\cos^{1/8}\chi]\,f(\lambda)\,f(z), \qquad \cos\chi > 0,$$

$$\text{Night} \qquad T_e(z) = 2000\,[1 - .3\,|\cos\chi|^{1/4}]\,f(\lambda)\,f(z), \qquad \cos\chi < 0, \tag{9}$$

$$f(\lambda) = \left[1 - .4\cos\left(\frac{3\lambda}{2}\right)\right],$$

and f(z) gives the altitudinal factor. Figure 1 shows the diurnal and altitudinal variations of T_e for Millstone Hill, Massachussetts (along L = 3.2) as given by these expressions. The ion temperature T_i is assumed to increase linearly with altitude from T_n to T_e between 400 km and 1000 km.

Table 1. Reaction Rates

Reaction	Reaction Rate ($cm^3\ s^{-1}$)	Reference
Ion-Neutral Charge Transfer Reactions		
$H^+ + O \rightarrow H + O^+$	$3.8 \times 10^{-11}(T_i + T_n/16)^{1/2}$	Schunk and Walker (1972)
$O^+ + H \rightarrow O + H^+$	$4.3 \times 10^{-11}(T_n + T_i/16)^{1/2}$	"
$O^+ + N_2 \rightarrow N + NO^+$	$1.2 \times 10^{-12}(300/T_i)$	"
$O^+ + O_2 \rightarrow O + O_2^+$	$2.0 \times 10^{-11}(300/T_i)^{1/2}$	"
Ion-Electron Radiative Recombination Reactions		
$O^+ + e^- \rightarrow O + h\nu$	$3.7 \times 10^{-12}(250/T_i)^{.7}$	Bates and Dalgrano (1962)
$H^+ + e^- \rightarrow H + h\nu$	$4.8 \times 10^{-12}(250/T_i)^{.7}$	"

Table 2. Collision Frequencies

Collision Frequency (s^{-1})	Reference
Ion-Neutral Collision Frequencies	
$\nu_{O^+-H} = 1.5 \times 10^{-12}\ T_n^{1/2} N_H$	Banks and Kockarts (1973)
$\nu_{H^+-O} = 2.1 \times 10^{-11}\ T_i^{1/2} N_O$	"
$\nu_{O^+-O} = 1.6 \times 10^{-11}\ (T_i + T_n)^{1/2} N_O$	Banks (1966)
$\nu_{H^+-H} = 1.0 \times 10^{-10} (T_i + T_n)^{1/2} N_H$	"
Ion-Ion Collision Frequencies	
$\nu_{O^+-H^+} = 7.88 \times 10^{-2}\ T_i^{-3/2} N_{H^+}$	Banks and Kockarts (1973)
$\nu_{H^+-O^+} = 1.26\ T_i^{-3/2} N_{O^+}$	"

The above quantities are not altered in the various model studies. The quantities that are adjusted are the neutral atmospheric densities and photoionization production rates. The neutral atmospheric densities of N_2, O_2 and O are calculated from the Jacchia (1964) model as presented by Walker (1965). The density of atomic hydrogen is obtained from the expression

$$N_{120}(H) = 1.7 \times 10^6 \left[1 + 0.3 \sin \frac{2\pi t}{86400}\right] cm^{-3},$$

so that the densities at 350 km agree with the observations of Brinton and Mayr (1971). The photoionization production rates are calculated by the theory of Chapman (1931 a, b). Different combinations of the model atmospheric parameters have been used in order to obtain the best possible results. These parameters are summarized in Table 3.

Two other important quantities that are prescribed are the meridional neutral wind and the vertical electromagnetic drift. The neutral wind model used in this study is given by

$$\text{Day} \qquad U = -40 \sin (\Lambda - \delta \cos\chi) \cos\chi \, ms^{-1}, \qquad \cos\chi > 0,$$

$$\text{Night} \qquad U = -120 \sin (\Lambda - \delta \cos\chi) \cos\chi \, ms^{-1}, \qquad \cos\chi < 0. \tag{10}$$

Figure 2 shows the diurnal variation of the neutral wind velocity for selected latitudes under equinox conditions.

The vertical electromagnetic drift velocity is specified by its equatorial value

$$V_{P_e} = \frac{\partial r_e}{\partial t} \ . \tag{11}$$

By integrating and dividing by r_o, we get the equation of motion of the tube of ionization under the action of the electromagnetic drift.

$$L(t) = L_o + \frac{1}{r_o} \int V_{P_e} dt \ . \tag{12}$$

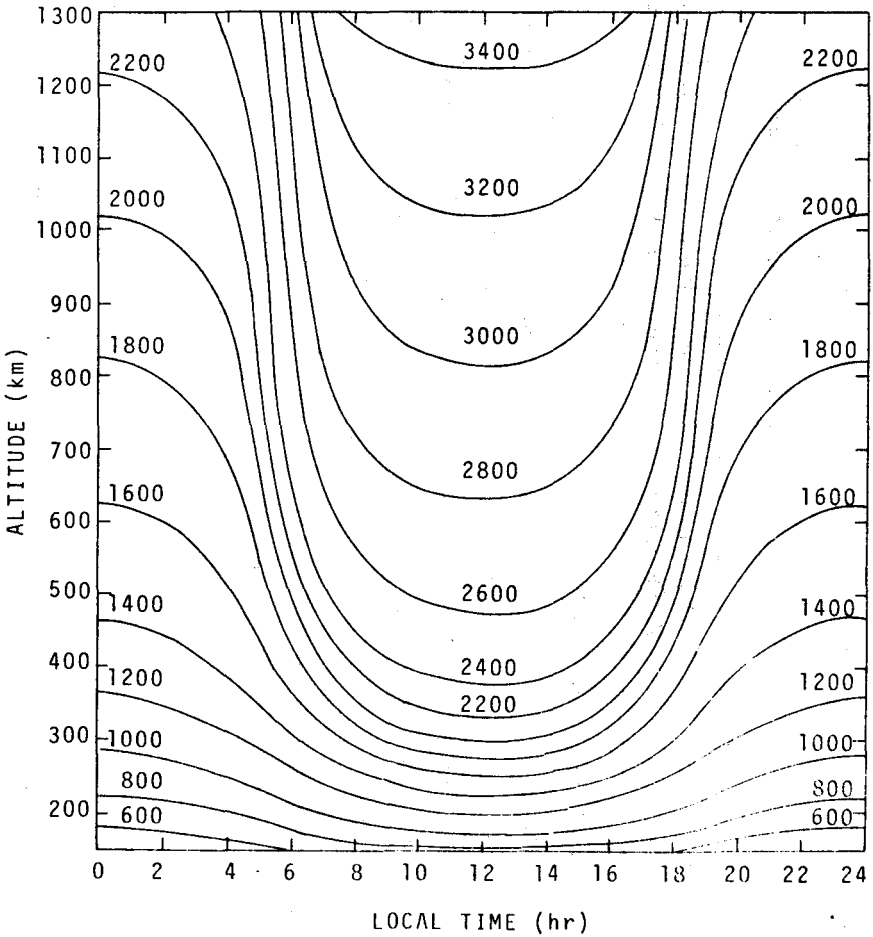

Fig. 1. Model diurnal and altitudinal variations of T_e at Millstone Hill for equinox conditions.

Table 3. Atmospheric Parameters

	Mid-latitude Profile Studies	Arecibo Profiles for February 10, 1972	Low-latitude Profile Studies	Ootacamund Profiles for December, 1975
Neutral Atmospheric Model				
Model	Jacchia (1971)	Jacchia (1971)	Jacchia (1970)	Jacchia (1970)
T_∞	800°K	800°K	775°K	750°K
$N_{120}(N_2)$	3.69×10^{11} cm^{-3}	3.69×10^{11} cm^{-3}	3.6×10^{11} cm^{-3}	3.6×10^{11} cm^{-3}
$N_{120}(O_2)$	5.20×10^{10} cm^{-3}	5.20×10^{10} cm^{-3}	5.0×10^{10} cm^{-3}	5.0×10^{10} cm^{-3}
$N_{120}(O)$	1.44×10^{11} cm^{-3}	1.44×10^{11} cm^{-3}	7.6×10^{10} cm^{-3}	7.6×10^{10} cm^{-3}
Ionization Rate Coefficients				
for O^+	2.5×10^{-7} s^{-1}	3.2×10^{-7} s^{-1}	4.5×10^{-7} s^{-1}	3.6×10^{-7} s^{-1}
for H^+	8.0×10^{-8} s^{-1}	1.1×10^{-7} s^{-1}	1.5×10^{-7} s^{-1}	1.2×10^{-7} s^{-1}

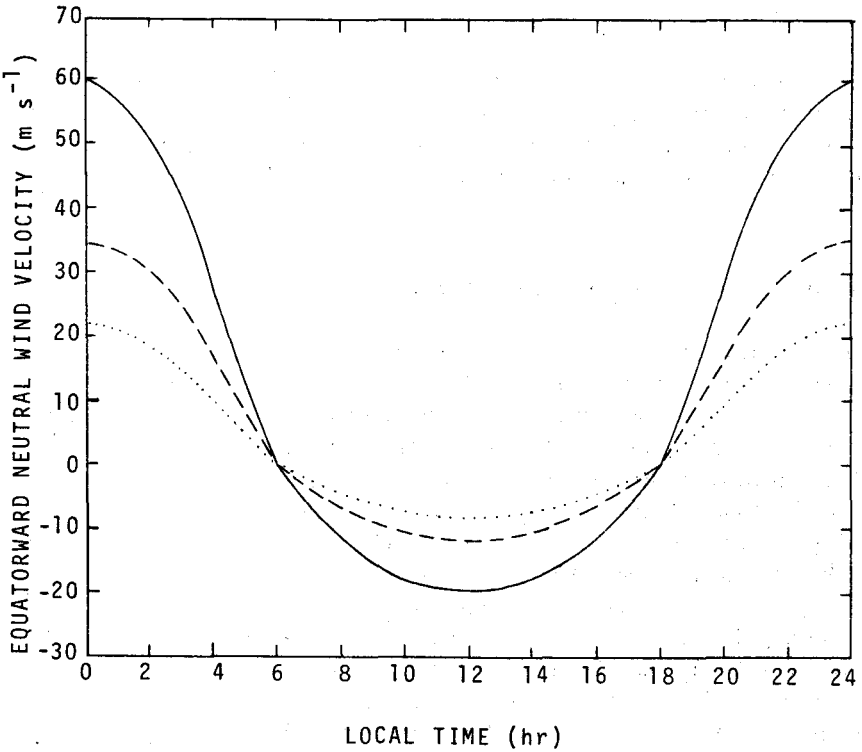

Fig. 2. Model equatorward neutral wind velocity at Millstone Hill (solid line), Arecibo (dashed line), and Jicamarca (dotted line) for equinox conditions.

4. RESULTS

This study investigates the main features of the mid- and low-latitude F region ionosphere and the protonosphere. In particular, model variations of the peak electron density ($N_m F2$), the height of the F2 peak ($H_m F2$), the $O^+ - H^+$ transition height (H_{tr}) and the transition level ion density of either O^+ or H^+ (N_{tr}) are studied.

4.1. *Mid-latitude ionospheric profile studies*

Model variations of $N_m F2$, $H_m F2$, N_{tr} and H_{tr} under sunspot minimum and equinox conditions at Arecibo ($\Lambda = 18.50^o$, $\Phi = 293.17^o$) are presented in Figure 3. The atmospheric parameters used are given in Table 3. The neutral wind model is given by equations (10) while a sinusoidal electromagnetic drift of amplitude 20 ms^{-1} is used. In the absence of electric fields and neutral winds, the results are readily explained. There is a sharp increase of $N_m F2$ at sunrise and a steady decline during the night. In the absence of electric fields and neutral winds, the height of the F2 peak remains near 300 km during the night. After sunrise, $H_m F2$ dips to near 250 km altitude where photoionization production maximizes. $H_m F2$ slowly rises during the day with upward diffusion of the ionization. This upward diffusion of O^+ immediately raises H_{tr} to above 1500 km and is accompanied by the steady conversion of O^+ to H^+. The variation of N_{tr} points to an upward flux of O^+ throughout the day and a downward flux throughout the night. The effect of the $E \times B$ drift on $N_m F2$ and $H_m F2$ is rather small at this latitude. The upward drift in daytime slightly diminishes $N_m F2$ due to greater spreading of ionization over higher altitudes. The effect of the downward drift during the night is also to decrease $N_m F2$ shifting the field tube slightly downward into regions of greater loss rate. The effect of the upward drift on $H_m F2$ becomes significant in the evening only, while H_{tr} shows a rapid rise in the morning hours.

The neutral wind is seen to have a much greater effect on $N_m F2$ than the electromagnetic drift. A poleward wind during the day drives the ionization to lower heights where greater loss reduces the peak electron density. The nighttime wind, on the other hand, drives the ionization to higher altitudes where loss rate is slower and reduces the decay of $N_m F2$. The neutral wind therefore has a stabilizing effect on $N_m F2$. The notion of the maintenance of the nocturnal $N_m F2$ at mid-latitudes by neutral winds (Hanson and Patterson, 1964) is realized in Figure 3. The effect of the neutral wind is also seen to flatten the gradients of the N_{tr} and H_{tr} curves, contrary to the effects of the electric field. The variation of H_{tr} with neutral wind generally follows the pattern deduced by Titheridge (1976), but with a greater amplitude.

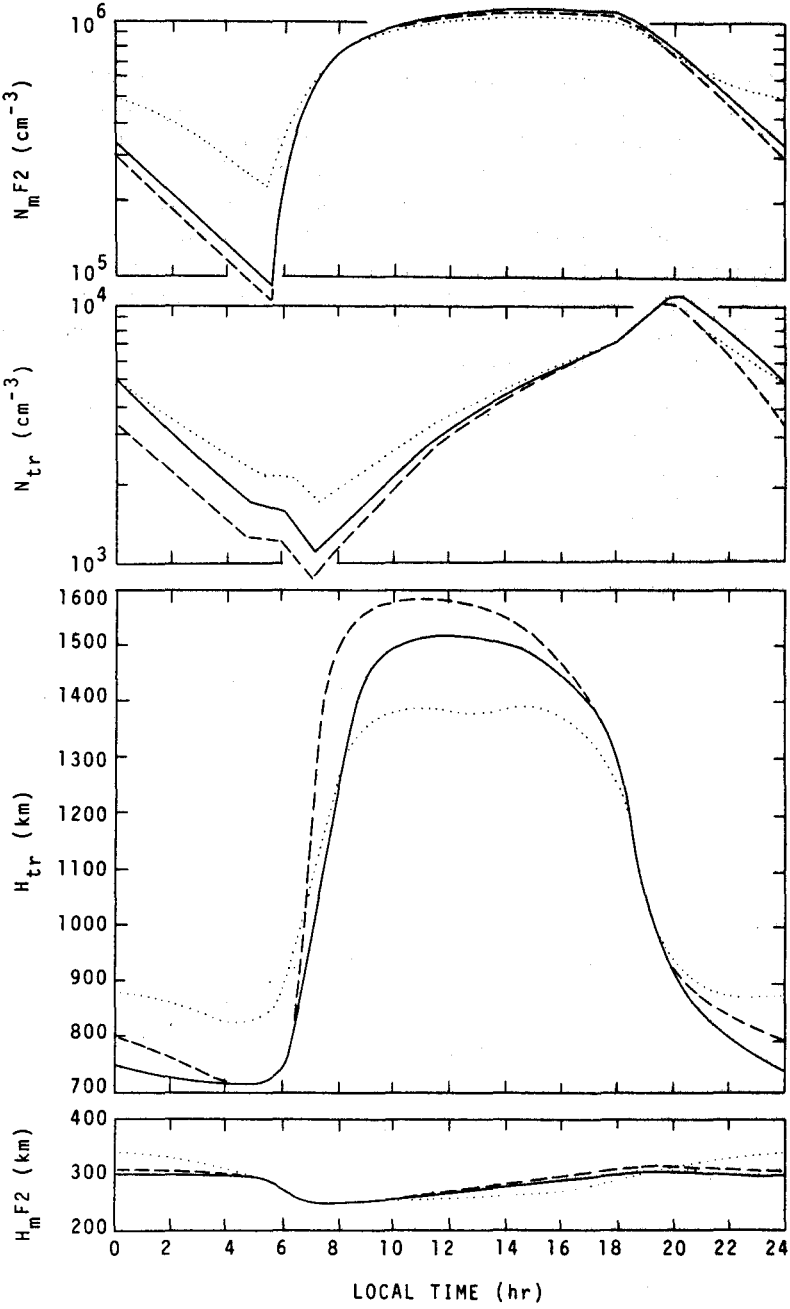

Fig. 3. Diurnal variations of N_mF2, H_mF2, N_{tr} and H_{tr} with no neutral wind or electric field (solid lines), with electric field but no neutral wind (dashed lines) and with neutral wind but no electric field (dotted lines) at Arecibo for sunspot minimum and equinox conditions.

Figures 4 and 5 show a few comparisons between observed and calculated ionospheric profiles at Millstone Hill ($\Lambda = 42.60^{o}$, $\Phi = 288.50^{o}$) and Arecibo. The Millstone Hill calculations were made for sunspot minimum and equinox conditions. The ion transition height lies above 1100 km and the H^+ density is rather small at this latitude. For the Arecibo profiles, higher photoionization rate coefficients were used (Table 3) and δ was taken to be -14.70^{o}. The best results were obtained with a moderately large E x B drift and a small neutral wind. The amplitude of the E x B drift was taken as 30 ms^{-1} while those of the meridional wind in equations (10) were halved. The observed densities in Figure 5 were taken from Hagen and Hsu (1974) with neglect of He^+ densities.

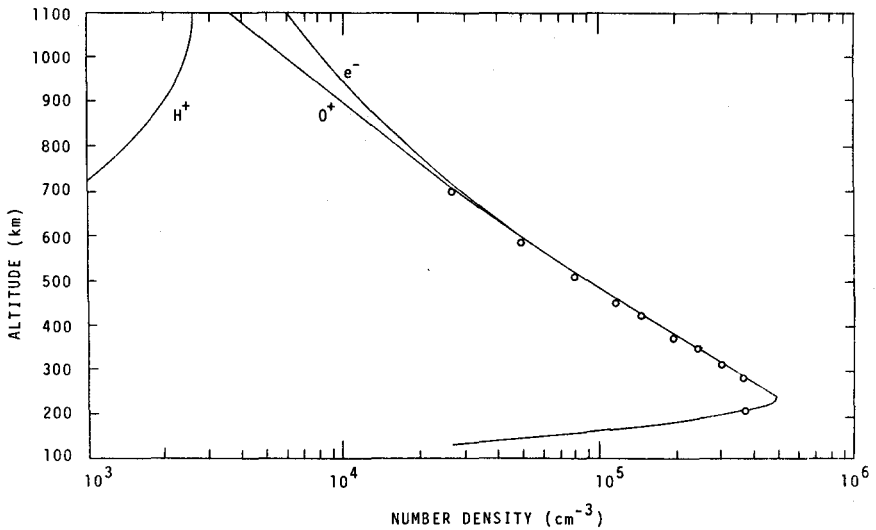

Fig. 4. Observed (circles, from Evans, 1967) and calculated electron densities at Millstone Hill for April, 1964 at 1400 LT.

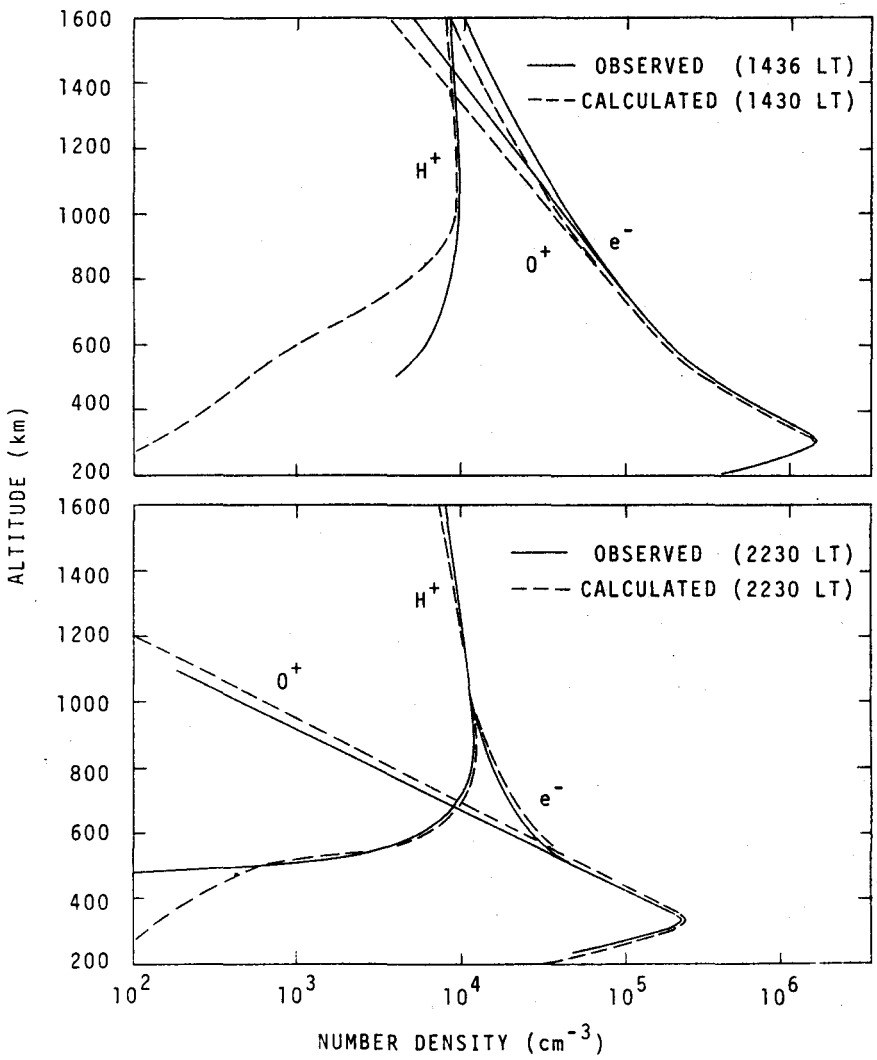

Fig. 5. Observed (solid lines, from Hagen and Hsu, 1974) and calculated (broken lines) electron and ion density profiles at Arecibo on February 10, 1972.

4.2. *Low-latitude ionospheric profile studies*

Figure 6 presents the calculated variations of $N_m F2$, $H_m F2$, N_{tr} and H_{tr} for equinox conditions at Jicamarca ($\Lambda = -11.95^o$, $\Phi = 283.14^o$) under simple drift velocity models. The model atmospheric parameters (Table 3) are chosen for later comparison with Ootacamund profiles. For the case of zero drift, the ionospheric profile shows rather simple diurnal variations that are readily explained for the idealized situation. $N_m F2$ builds up after sunrise and the F2 peak is situated near 320 km. During the night, the higher loss rate of O^+ at this altitude diminishes the O^+ density there and consequently $H_m F2$ migrates to a higher altitude of about 400 km. The enhancement of O^+ also drives H_{tr} to higher altitudes during the day. The broken lines show the case of an idealized sinusoidal drift velocity model with amplitude of 20 ms^{-1}. A characteristic result of such drift models is the formation of two distinct peaks in the $N_m F2$ curve, separated by a 'valley'. A manifestation of the 'equatorial anomaly', this phenomenon is called the 'noon bite-out' and is a common occurrence in the low-latitude $N_m F2$ curves around the world. Subsequent to Martyn's (1947) explanation of the equatorial anomaly, this phenomenon has been investigated by Bramley and Peart (1965), Hanson and Moffett (1966), and Baxter and Kendall (1968). The model sinusoidal drift velocity raises tubes of ionization during the day and lowers them during the night, thereby altering both $H_m F2$ and H_{tr} curves after itself. There is a marked increase in N_{tr} after sunset, when the direction of the drift is reversed. The dotted lines represent the case of a 'rift valley' shaped drift model. In this model, the upward drift is constant from 0800 LT to 1600 LT. The resulting $N_m F2$ curve has the shape of a plateau for daytime hours. $H_m F2$, however, has a gradual rise during the day. N_{tr} has a pattern similar to that of the sinusoidal drift but H_{tr} has a more 'plateau'-like shape. The higher density at the transition altitude after sunset is present with both the sinusoidal and the 'rift-valley' shaped drift models. This follows the beginning of the downward drift of ionization. As H_{tr} decreases, N_{tr} increases until after the F region has decayed substantially and downward fluxes begin to reduce N_{tr}.

The dotted and dashed lines illustrate an interesting case where the drift velocity has two peaks separated by two valleys. The higher peak is located at 1000 LT and the lower one at 2000 LT. In this case, the daytime 'bite-out' in $N_m F2$ occurs earlier because of the greater initial upward drift. Again, both H_{tr} and $H_m F2$ curves are strongly influenced by the drift pattern, with the second peak in $H_m F2$ higher than the first. The post-sunset increase in N_{tr} is suppressed and delayed by the second upward drift during this time. Another interesting feature of the 'double-peaked' drift model is the enhancement in $N_m F2$ after midnight. At this time the drift velocity is downwards and the F2 peak is situated above 350 km. Evidently, the enhancement took place in a loss region when the 'squeezing' of the field tubes associated with the downward drift overcame the loss rate of O^+. This can be view-

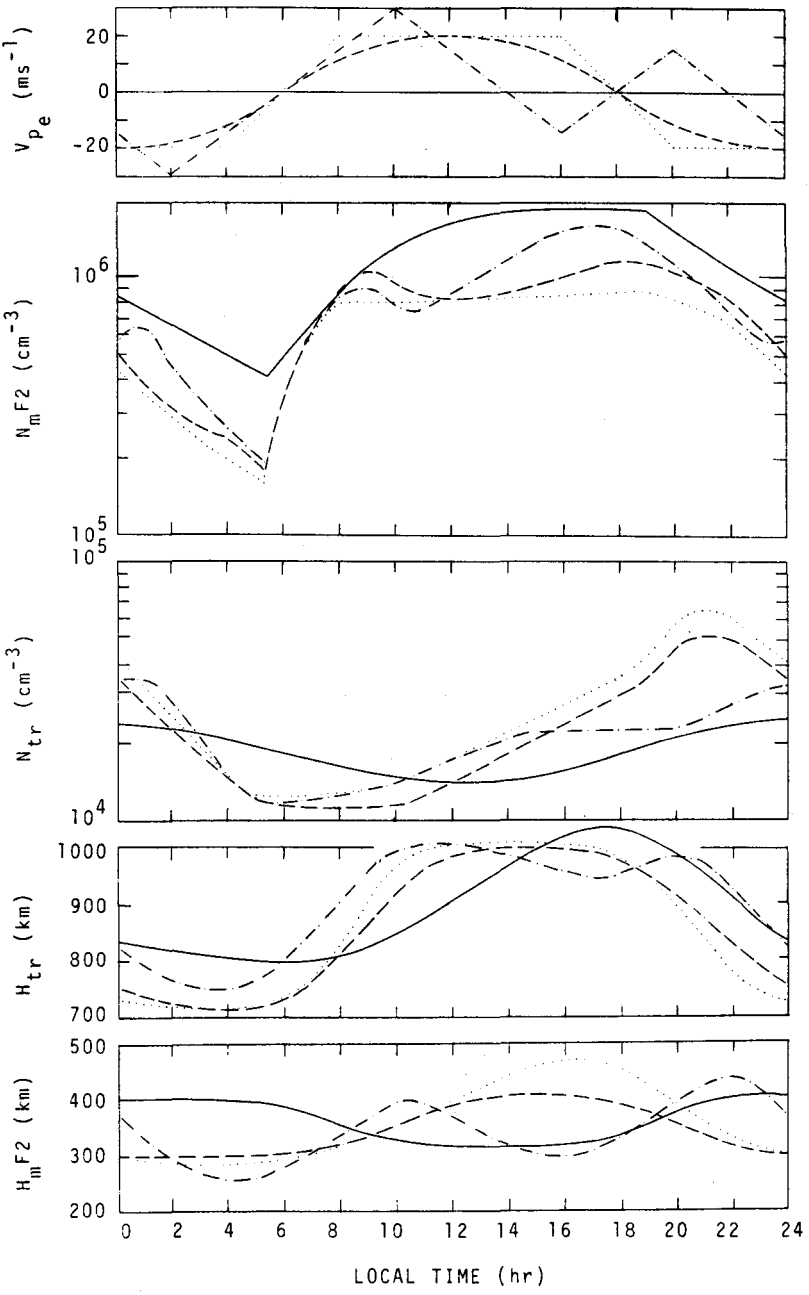

Fig. 6. Diurnal variations of N_mF2, H_mF2, N_{tr} and H_{tr} for the cases of no drift (solid lines), sinusoidal drift (dashed lines), 'rift-valley' shaped drift (dotted lines) and 'double-peaked' drift velocity models (dotted and dashed lines).

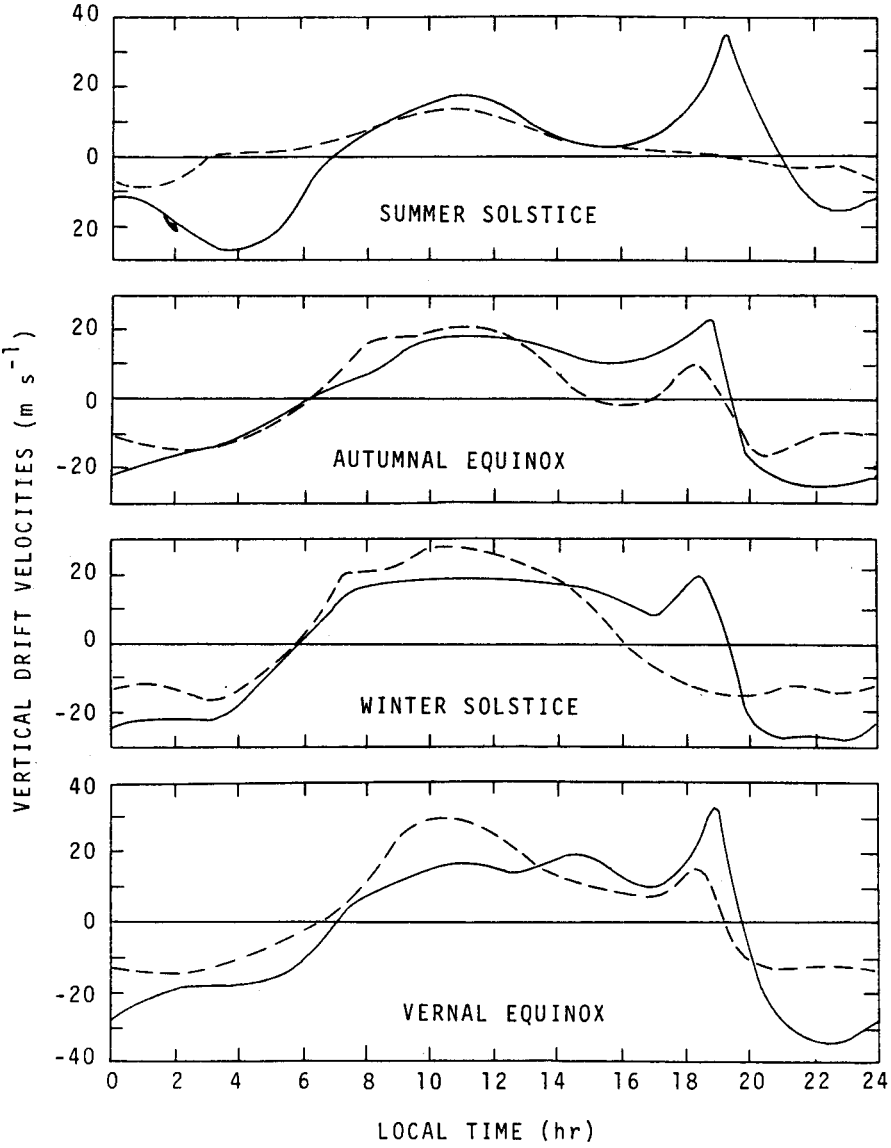

Fig. 7. F region vertical drift velocities at Jicamarca for 1968-69 (solid lines) and 1975-76 (dashed lines).

ed as the reverse of the daytime 'bite-out'. Occurrences like this were observed at Ibadan and Kodaikanal (cf. Rastogi and Sanatani, 1963).

While the drift velocity models considered were idealized cases, the results are nevertheless valuable in understanding the nature of ionospheric response to the various drifts. This would become evident in the following study of the Ootacamund profiles. The real drifts observed over Jicamarca (Figure 7, from R. F. Woodman, unpublished) were similar to those chosen for our study.

4.3 *Total electron content studies at Ootacamund*

By total electron content N_T is meant the total number of electrons in a tube of unit cross section along the raypath. It is thus equal to the area under the electron density curve along the raypath. Modulation phase measurements of the ATS-6 radio beacon experiments have furnished, for the first time, the total electron content from ground to the satellite (Davies *et al.*, 1976). Figure 8 (from Bouwer *et al.*, 1979) shows the total electron contents from Ootacamund to the ATS-6 satellite for the months of October, November and December, 1975. Progressive diminution of the content is evident as the months approach winter. The objective of this study is to find a plausible drift velocity model that, together with suitable atmospheric parameters, would simulate the observed results.

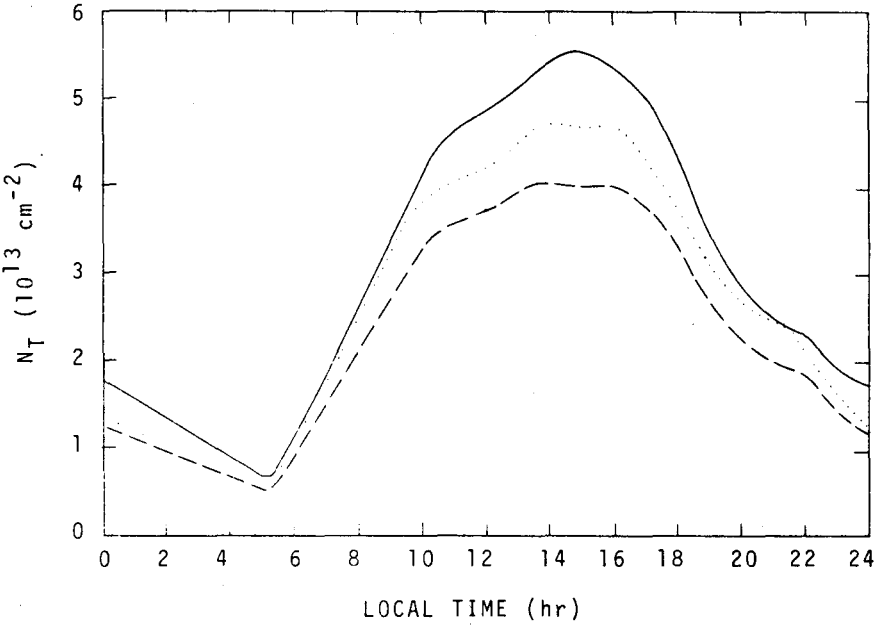

Fig. 8. Median values of the total electron content from Ootacamund to the ATS-6 satellite for the months of October (solid line), November (dotted line) and December (dashed line), 1975 (from Bouwer *et al.*, 1979).

Ootacamund ($\Lambda = 11.25^{o}$, $\Phi = 76.43^{o}$), like Jicamarca, is situated near the geomagnetic equator, while the ATS-6 satellite, in its second phase, was located at ($\Lambda = 0^{o}$, $\Phi = 35^{o}$). In order to study the total electron content along a slant raypath, we need to find the electron densities along the raypath and integrate them up to the plasmapause at which the ion density drops to zero. This is done by running the program for a host of field lines covering the region up to the plasmapause. The densities along the raypath are determined by two interpolation schemes. The first interpolates the densities along the zenith angle θ and the second interpolates the densities along the local time. Finally, an integration scheme yields the total content along the slant path. Since the plasmasphere normally extends up to about L = 4.5 (Maynard and Grebowsky, 1977), it suffices to integrate the electron densities up to L = 5.

In modelling the total content, the ionospheric profile is of importance, since it is possible that different profiles can have the same content. For this reason, parameters such as $N_m F2$ and $H_m F2$ have to be taken into consideration. Because of the lack of $N_m F2$ and $H_m F2$ data at Ootacamund, we have looked for those at neighboring stations. The median values of $N_m F2$ are obtained from the $f_o F2$ data of Kodaikanal ($\Lambda = 10.20^{o}$, $\Phi = 77.50^{o}$), whereas the median values of $H_m F2$ are taken from the HPF2 data of Thumba ($\Lambda = 8.60^{o}$, $\Phi = 76.90^{o}$). The atmospheric parameters (Table 3) were so chosen as to obtain reasonably good fits with the observed data. The drift velocity models for October and December and the results of the calculations are shown in Figures 9 and 10. The declinations of the sun for the two months were taken as -8.2^{o} and -23.22^{o}, respectively.

In arriving at our model drifts, the following points were taken into consideration.

(1) For the month of October, $N_m F2$ shows two distinct 'bite-outs' during the day. This indicates the presence of two separate upward drifts, one occurring around 1000 LT and the other around 1900 LT. For the month of December, the first 'bite-out' has given way to a near plateau, which points to a steady upward drift.

(2) The steady decline of $N_m F2$ during the night suggests steady downward drifts during the night rather than a large downward drift that produces an enhancement in $N_m F2$.

(3) The variation of $H_m F2$ supports our contentions (1) and (2) and is consistent with the $N_m F2$ data.

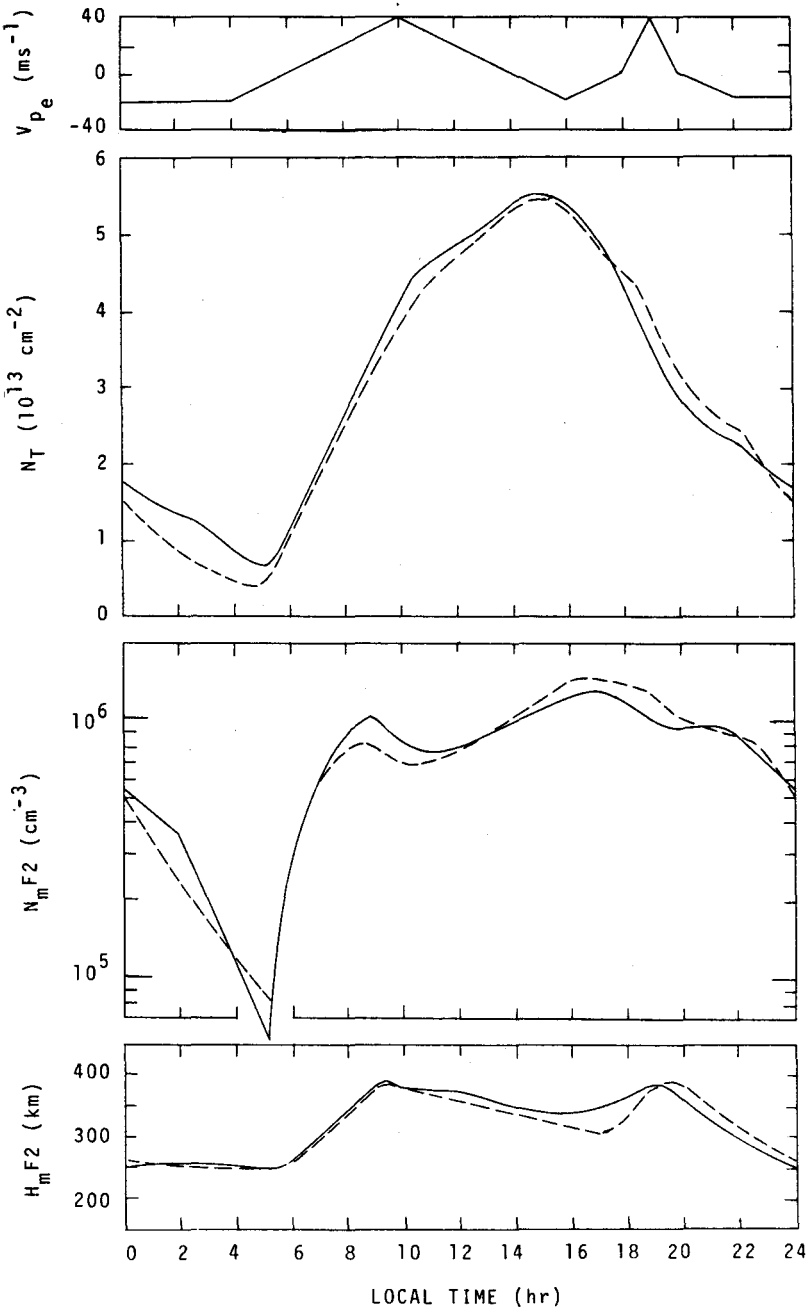

Fig. 9. Vertical drift velocity model at Ootacamund for October 1975, and the resulting diurnal variations of N_T, N_mF2 and H_mF2. The solid lines in the N_T, N_mF2 and H_mF2 diagrams represent the observed values.

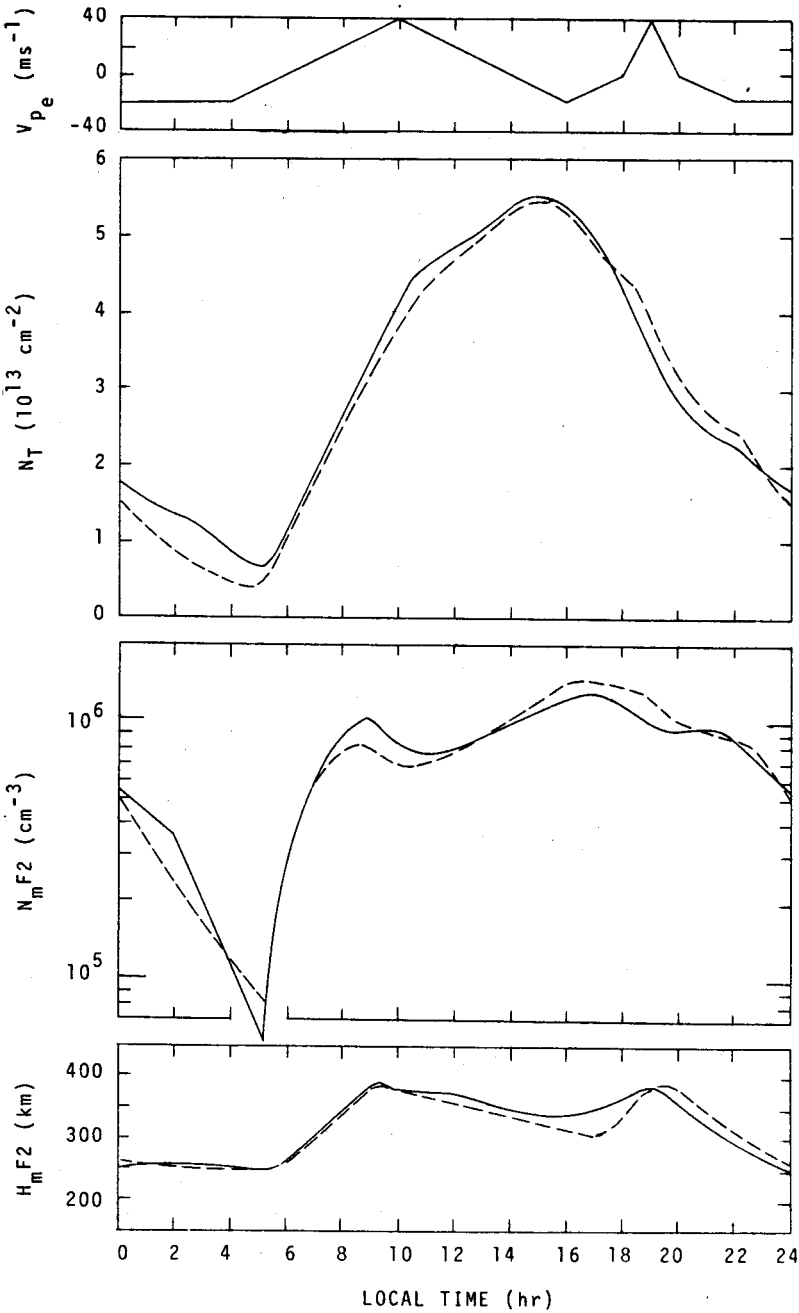

Fig. 9. Vertical drift velocity model at Ootacamund for October 1975, and the resulting diurnal variations of N_T, N_mF2 and H_mF2. The solid lines in the N_T, N_mF2 and H_mF2 diagrams represent the observed values.

(4) The early morning 'rise' in $N_m F2$ and N_T give a measure of the production rates.

(5) An upward drift in daytime (which decreases $N_m F2$) increases N_T because of the lifting of the ionization produced to higher heights where loss rates are smaller . Conversely, a downward drift during the day decreases N_T, although it increases $N_m F2$.

(6) Downward drifts during the night decrease N_T while they may increase or decrease $N_m F2$ depending upon the drift velocity.

It is emphasized that the drift velocity models are not those giving the closest possible fits with the experimental data. Rather, they represent simple drift velocity models that adequately and simultaneously explain the main features of N_T, $N_m F2$ and $H_m F2$. The fairly good agreement between observed and calculated results indicates that the model drifts were quite realistic. It also indicates consistency between the N_T, $N_m F2$ and $H_m F2$ measurements over the three nearby locations (Ootacamund, Kodaikanal and Thumba). Comparisons with Figure 7 reveal broad similarities between the vertical drifts at Jicamarca and Ootacamund. In the year 1975, the Jicamarca drifts show very little or no sunset maxima. If we compare the Autumn drifts with the October drifts at Ootacamund, we find a much larger sunset maximum at Ootacamund. Otherwise both drifts show a small downward motion near 1600 LT and a fairly constant downward motion during the night. During the winter, the Jicamarca observations show a large upward drift in daytime and a total absence of the sunset maximum, whereas the Ootacamund drift stays constant during the day and has a small sunset maximum. During the night, however, both drifts are downward.

Difficulty was encountered in fitting the October and December data with the same atmospheric parameters. The total content was 40 % greater in October than in December and this could not be explained in the model by merely changing the declination of the sun and the resulting changes in the neutral atmospheric densities and production rates. The production rates had to be increased considerably for October to obtain better agreement with observations. However, this does not seriously affect the determination of the drifts, which strongly affect the $N_m F2$ and $H_m F2$ variations. It appears that the key to this discrepancy lies in the neutral atmospheric model. The seasonal variations in the neutral atmospheric densities are greater than those allowed by the static diffusion model of Jacchia (cf. Jacchia, 1974). This problem needs further investigation in the future.

5. CONCLUSIONS

The time dependent continuity and momentum equations of O^+ and H^+ are solved for both mid- and low-latitude locations. The effect of a sinusoidal E x B drift at mid-latitudes is to accentuate the gradients of the $N_m F2$, $H_m F2$, N_{tr} and H_{tr} curves , whereas a nighttime equatorward neutral wind acts to stabilize the ionospheric profile by reducing the variations of $N_m F2$, N_{tr} and H_{tr}.

The electromagnetic drift plays a dominating role in the low-latitude ionosphere. A vertical drift that peaks during the day produces a 'valley' in the $N_m F2$ curve, while a constant vertical drift produces a 'plateau'. The nighttime decay of $N_m F2$ is a result of a slow downward drift and ion recombination. A nocturnal increase in $N_m F2$ occurs in a low loss region with a sufficiently large downward drift. The $H_m F2$ and H_{tr} variations tend to follow the drift velocity pattern with gradients somewhat flattened. A downward reversal of the drift at sunset causes an enhancement in the post-sunset N_{tr}.

Application of the model to the N_T, $N_m F2$ and $H_m F2$ studies provides a determination of the vertical drift velocity over Ootacamund. The drift velocity pattern shows broad similarities and minor differences with those observed over Jicamarca.

APPENDIX

List of Symbols

N = number density
V = velocity
B = earth's magnetic field
t = local time
s = arc length along geomagnetic field lines from the base of the ionosphere in the northern hemisphere
α = production rate of ions
β = loss coefficient of ions
k = Boltzmann's constant
T = temperature
e = electronic charge
E = electric field
m = ion mass
g = acceleration due to gravity
ν = collision frequency
u = meridional neutral wind velocity (reckoned positive, if equatorward)
f = centrifugal acceleration
G = universal gravitational constant
M = mass of the earth
Ω = angular velocity of the earth
V_{P_e} = equatorial value of the vertical drift velocity
L = McIlwain's shell parameter
r = radial coordinate
r_e = equatorial value of r
r_0 = radius of the earth
θ = dipole colatitude
Θ = geographic colatitude
λ = dipole latitude
Λ = geographic latitude
Φ = geographic longitude
Θ_0 = geographic colatitude of geomagnetic north pole
δ = declination of the sun
χ = solar zenith angle
z = altitude
T_∞ = exospheric neutral temperature

Coefficients of the Diffusion Equations

$$P_i' = X_i$$

$$Q_i' = B \frac{\partial}{\partial s} \left(\frac{X_i}{B} \right) + Y_i$$

$$R_i' = B \frac{\partial}{\partial s} \left(\frac{Y_i}{B} \right) - \nabla \cdot \vec{V}_\perp - \beta_i$$

$$S_i' = \alpha_i$$

$$X_i = \frac{\nu_j k T_i}{\nu_{m_i}} + \left(\frac{\nu_{ij}}{\nu_{m_j}} + \frac{\nu_j}{m_i} \right) \frac{k T_e N_i}{N_e}$$

$$Y_i = \left(\frac{\nu_{ij}}{\nu_{m_j}} + \frac{\nu_j}{\nu_{m_j}} \right) k \frac{\partial}{\partial s} (T_i + T_e)$$

$$+ \left\{ \left(\frac{\nu_{ij}}{\nu_{m_j}} + \frac{\nu_j}{\nu_{m_j}} \right) \frac{k T_e}{N_e} + \frac{\nu_{ij}}{\nu_{m_j}} \frac{K T_i}{N_j} \right\} \frac{\partial N_j}{\partial s}$$

$$- \frac{\nu_{ij} + \nu_j}{\nu} (g_{||} + f_{||})$$

$$- \frac{\nu_{ij} \nu_{jo} + \nu_j \nu_{io}}{\nu} U_{||}$$

$$\nu = \nu_i \nu_j - \nu_{ij} \nu_{ji}$$

$$\nu_i = \nu_{io} + \nu_{ij}$$

$$\nu_{io} = \sum_n \nu_{in}$$

$$g_{||} = - \frac{2GM \sin\theta}{r_e^2 \sin^4\theta \, (3\cos^2\theta + 1)^{1/2}}$$

$$U_{||} = \frac{U(\cos\Theta_o - \cos\theta \cos\Theta)}{\sin\Theta \, (3\cos^2\theta + 1)^{1/2}}$$

$$f_{||} = \frac{3\Omega^2 r_e \cos\theta \sin^2\theta \, (1 - \cos^2\theta - \cos^2\Theta + \cos\theta \cos\Theta \cos\Theta_o}{(3\cos^2\theta + 1)^{1/2}}$$

$$\nabla \cdot V_\perp = \frac{6V_{P_e} \sin^2\theta \, (\cos^2\theta + 1)}{r_e (3\cos^2\theta + 1)^2}$$

$$\frac{d}{dt} \equiv \frac{\partial}{\partial t} + V_\perp \cdot \nabla$$

$$V_\perp = \frac{E \times B}{B^2}$$

$$P_i = \gamma^2 P_i'$$

$$Q_i = \gamma P_i' \frac{\partial \gamma}{\partial x} + \gamma Q_i'$$

$$R_i = R_i'$$

$$S_i = S_i'$$

$$\frac{\partial}{\partial s} \equiv \gamma \frac{\partial}{\partial x}$$

$$\gamma = - \frac{(3\cos^2\theta + 1)^{1/2} \Gamma \cosh(\Gamma_q)}{L^2 r_e \sin^6\theta \sinh(\Gamma q_{min})}$$

ACKNOWLEDGMENTS

The authors are grateful to Drs. R. F. Donnelly and D. N. Anderson of the National Oceanic and Atmospheric Administration for initiating this study and useful discussions throughout its course. We also acknowledge the collaboration of Dr. G. J. Bailey of the University of Sheffield with regard to the numerical aspects of the model. This work was conducted at NOAA Space Environmental Laboratory, Boulder, Colorado, and was partially supported by NASA Marshall Space Flight Center under Contract NAS 8-33443. The computations were done at the National Center for Atmospheric Research, Boulder, Colorado, which is sponsored by The National Science Foundation.

BIBLIOGRAPHY

ANDERSON, D. N., 1973. A theoretical study of the ionospheric F region equatorial anomaly. *Planet. Space Sci. 21,* pp. 409-422.

ANGERAMI, J. J. and J. O. THOMAS, 1964. Studies of planetary atmospheres. *J. Geophys. Res. 69,* pp. 4537-4550.

BANKS, P. M., 1966. Collision frequencies and energy transfer - ions. *Planet. Space Sci. 14,* pp. 1105-1122.

BANKS, P. M. and G. KOCKARTS, 1973. Aeronomy. *Academic Press,* New York.

BATES, D. R. and A. DALGARNO, 1962. Atomic and Molecular Processes, *Academic Press,* New York.

BAXTER, R. G. and P. C. KENDALL, 1968. A theoretical technique for evaluating time-dependent effects of general electrodynamic drifts in the F2 layer of the ionosphere. *Proc. Roy. Soc. A304,* pp. 171-180.

BOUWER, S. D., K. DAVIES, R. F. DONNELLEY, R. G. RASTOGI and M. R. DESHPANDE, 1979. ATS-6 radio beacon electron content measurements at Ootacamund, India. World Data Center A for Solar Terrestrial Physics, UAG Report.

BRAMLEY, E. N. and M. PEART, 1965. Diffusion and electromagnetic drift in the equatorial F2 region. *J. Atmos. Terr. Phys. 27,* pp. 1201-1211.

BRINTON, H. C. and H. G. MAYR, 1971. Temporal variations of thermospheric hydrogen derived from in situ measurements, *J. Geophys. Res. 76,* pp. 6198-6201.

CHAPMAN, S., 1931a. The absorption and dissociative or ionizing effect of monochromatic radiation in an atmosphere on a rotating earth. *Proc. Phys. Soc. (London) 43,* pp. 26-45.

CHAPMAN, S., 1931b. The absorption and dissociative or ionizing effect of monochromatic radiation in an atmosphere on a rotating earth. II. Grazing incidence. *Proc. Phys. Soc. (London) 43,* pp. 483-501.

DAVIES, K., R. B. FRITZ and T. B. GRAY, 1976. Measurements of the columnar electron content of the ionosphere and plasmasphere, *J. Geophys. Res. 81,* pp. 2825-2834.

EVANS, J. V., 1967. Midlatitude F region densities and temperatures at sunspot minimum. *Planet Space Sci. 15,* pp. 1387-1405.

HAGEN, J. B. and P. Y. S. HSU, 1974. The structure of the protonosphere above Arecibo. *J. Geophys. Res. 79,* pp. 4269-4275.

HANSON, W. B. and R. J. MOFFET, 1966. Ionization transport effects in the equatorial F region. *J. Geophys. Res. 71,* pp. 5559-5572.

HANSON, W. B. and T. N. L. PATTERSON, 1964. The maintenance of the nighttime F layer, *Planet. Space Sci. 12,* pp. 979-997.

JACCHIA, L. G., 1964. Static diffusion models of the upper atmosphere with empirical temperature profiles. Smithsonian Astrophys. Obs. Spec. Rept. *170.*

JACCHIA, L. G., 1970. New static models of the thermosphere and exosphere with empirical temperature profiles. Smithsonian Astrophys. Obs. Spec. Rept. *313.*

JACCHIA, L. G., 1971. Revised static models of the thermosphere and exosphere with empirical temperature profiles. Smithsonian Astrophys. Obs. Spec. Rept. *332.*

JACCHIA, L. G., 1974. Variations in thermospheric composition: A model based on mass spectrometer and satellite drag data. *J. Geophys. Res. 79,* pp. 1923-1927.

KENDALL, P. C., 1962. Geomagnetic control of diffusion in the F2-region of the ionosphere. I. The form of the diffusion operator. *J. Atmos. Terr. Phys. 24,* pp.805-811.

LAASONEN, P., 1949. Uber eine methode zur lösung der wärmeleitungsgleichung. *Acta Math. 81,* pp. 309-317.

MARTYN, D. F., 1947. Atmospheric tides in the ionosphere. 1. Solar tides in the F2 region, *Proc. Roy. Soc.* A189, pp. 241-260.

MASSA, J., 1974. Theoretical and experimental studies of the ionization exchange between the ionosphere and the plasmasphere, Ph. D. Thesis, University of Michigan.

MAYNARD, N. C. and J. M. GREBOWSKY, 1977. The plasmapause revisited, *J. Geophys. Res. 82,* pp. 1591-1600.

MAYR, H. G., E. G. FONTHEIM, L. H. BRACE, H. C. BRINTON and H. A. TAYLOR, Jr., 1972. A theoretical model of the ionospheric dynamics with interhemispheric coupling, *J. Atmos. Terr. Phys. 34,* pp. 1659-1680.

MOFFETT, R. G. and J. A. MURPHY, 1973. Coupling between the F-region and protonosphere: Numerical solution of the time-dependent equations. *Planet Space Sci. 21,* pp. 43-52.

RASTOGI, R. G. and S. SANATANI, 1963. Longitudinal effects in the equatorial F2-region of the ionosphere. *J. Atmos. Terr. Phys. 25,* pp. 739-742.

RICHTMYER, R. D., 1957. Difference methods for initial-value problems. Interscience, New York.

SCHUNK, R. and J. C. G. WALKER, 1972. Oxygen and hydrogen ion densities above Millstone Hill. *Planet. Space Sci. 20,* pp. 581-589.

STERLING, D. L., W. B. HANSON, R. J. MOFFETT and R. G. BAXTER, 1969. Influence of electromagnetic drifts and neutral air winds on some features of the F2 region, *Radio Science 4,* pp. 1005-1023.

TITHERIDGE, J. E., 1976. Ion transition heights from topside electron density profiles. *Planet. Space Sci. 24,* pp. 229-245.

WALKER, J. C. G., 1965. Analytic representation of upper atmosphere densities based on Jacchia's static diffusion models. *J. Atmos. Sci. 22,* pp. 462-463.